Leblouba *Advances in Bridge Engineering* (2022) 3:11
https://doi.org/10.1186/s43251-022-00062-1

Advances in
Bridge Engineering

ORIGINAL INNOVATION Open Access

Stability analysis of elastomeric bearings in bridge structures

Moussa Leblouba*

*Correspondence:
mleblouba@sharjah.ac.ae

Department of Civil & Environmental Engineering, College of Engineering, University of Sharjah, P.O.BOX 27272, Sharjah, UAE

Abstract

Elastomeric bearings (EB) and lead-rubber bearings (LRB) are used in bridge structures to reduce vehicle vibrations, wind loads, and earthquakes. Therefore, studying their stability is crucial to ensuring the stability of the bridge system itself. Building upon previously proposed linear and partially nonlinear models, two fully nonlinear models suitable for EBs and LRBs are proposed in this paper. The models are developed to adequately account for the interaction between the horizontal and vertical loads and their effect on the bearing's performance. This study considers that the horizontal and vertical loads do not always act in isolation and that their interaction can significantly affect the bearing's overall behavior and stability. Comparisons with experiments demonstrated that the models could accurately replicate the behavior of seismic isolators. Additionally, analytical models are developed to predict the horizontal and vertical stiffnesses as a function of the critical buckling load. The two mathematical models can readily be incorporated into open-source structural analysis software, such as OpenSees.

Keywords: Elastomeric bearing, Lead rubber bearing, Stability, Nonlinear model, Interaction, Stiffness

1 Introduction

Vibrations induce input energy to structures, and if they are not well isolated against vibrations, they may fail and cause catastrophic consequences. An example of a structure that withstood such fate includes the Onagawa nuclear power station (Ibrion et al. 2020). Vibration isolation and damping systems come in a variety of types. For instance, some use viscous damping to reduce vibrations due to friction (Graf and Lankenau 2021) and some use the concept of sloshing liquid tanks to reduce vibrations due to lateral loads such as wind and earthquake ground motions (Tsao and Huang 2021). The vibration isolation system uses both viscous damping and friction to reduce input energies originating from the vehicular and lateral loads in the bridge industry.

Most of the existing bridges use elastomeric bearings, which rely on rubber or synthetic elastomer to absorb the energy originating from vehicles, wind loads, earthquake ground motions, etc. These bearings come in two varieties: high damping rubber bearings (HDRB) and lead rubber bearings (LRBs). Other systems also exist, but they are not as commonly used.

(a) Steel bridge girder under construction (Image courtesy of Pam Broviak)

(b) Completed reinforced concrete bridge (Image courtesy of MAURER Germany)

Fig. 1 Elastomeric bearings installation in bridge structures

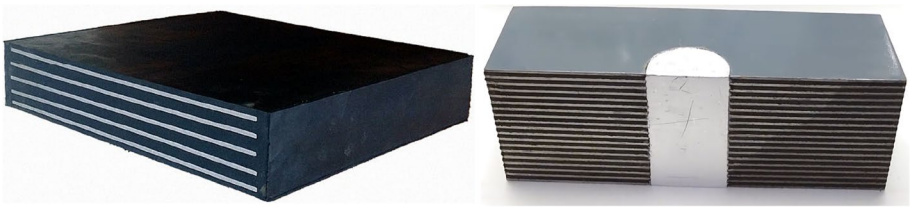

Fig. 2 Elastomeric bearing on the left and lead rubber bearing on the right (source: alibaba.com)

Elastomeric bearing pads are cost-effective to reduce noise and vibration in transportation applications. They are easy to install and do not require special tools or equipment. In addition, they are reusable and can be moved from one location to another as needed.

Figure 1 shows the installation of elastomeric bearings in a steel girder bridge under construction and a completed reinforced concrete bridge box with already installed rubber bearings.

The LRBs (Fig. 2) are a type of energy-absorbing isolation system that has been developed to increase the energy dissipation capacity of rubber bearings. It is widely used in New Zealand and consists of a steel-reinforced elastomeric bearing with a lead plug inserted in its center. The lead plug is firmly pressed into a hole in the center, and the lead forms a positive key between the steel plates within the bearing, which helps to confine them.

The effects of the lead core temperature on the performance of lead rubber bearings have been the subject of few studies. Kalpakidis and Constantinou (2009a) developed a theory for predicting the temperature rise of the lead core and the reduction in characteristic strength and energy dissipation history of lead-rubber bearings subjected to cyclic motion. The theory includes a simplified solution in which an explicit closed-form equation for the temperature rise was derived. The theory is useful in predicting the cyclic behavior of lead-rubber bearings for simplified analysis, extrapolating experimental data from one scale to another, and developing models for dynamic response history analysis of seismically isolated structures that account for the time-dependent mechanical properties of the bearings.

The authors' additional study (Kalpakidis and Constantinou 2009b) aimed to validate the theory presented in their previous research paper. The study used finite-element heat transfer analyses and experimental results from testing six different lead-rubber bearings. The study's results confirmed the theory's accuracy and showed that testing at quasi-static conditions results in a lesser increase in the lead core temperature and a lesser reduction of dissipated energy per cycle and characteristic strength of lead-rubber bearings. This difference in reduction in EDC is dependent on the geometry of the bearing, the conditions of testing, and the number of cycles imposed.

Kalpakidis et al. (2010) developed a model of the hysteretic behavior of lead rubber bearings that accounts for the temperature increase in the lead core based on first principles. The model can predict the lead core's instantaneous temperature and its instantaneous effect on the characteristic strength of the bearing. The paper demonstrates that the model is in good agreement with experimental results. The paper further uses the model to examine the effects of lead core heating on the dynamic response of an isolated structure. The study's results demonstrate that bounding analysis produces conservative results for predicting isolation system displacement demand, peak shear force, and peak structural responses.

The HDRB system is similar to the LRB system, but the rubber is thinner and has steel shims between the layers; this increases the vertical stiffness of the bearing while also allowing for a certain amount of lateral deformation. The LRB system uses thicker rubber sheets, which provide more lateral deformation, but also have a lower vertical stiffness.

Both types of bearings work by deflecting the energy from the earthquake away from the structure rather than absorbing it. This is done by making the structure vibrate at a frequency different from the earthquake's frequency. The isolation system does not work as well when there is high energy in the earthquake motion at frequencies close to the isolator's fundamental frequency. The MRPRA developed a natural rubber with enough inherent damping to overcome this issue. This damping is increased by adding extra-fine carbon block, oils or resins, and other proprietary fillers. The increased damping helps to suppress any possible resonance at the isolation frequency.

An isolator's lateral stiffness is minimal compared to its vertical stiffness, making it almost elastic for lateral deformations within its radius. This allows the isolator to easily deflect the energy from the earthquake, which keeps the structure safe.

Yuan et al. (2020) developed a new polyurethane elastomer (PUE) material with improved shear performance. This material was used to create isolation bearings with increased vertical capacity. The mechanical properties of the PUE material were investigated, and a rheological shear constitutive model was proposed. The accuracy of the proposed constitutive model was verified by the isolation bearings experimental. Results from the experimental investigations and a basic shear mechanical study of the new PUE material suggest that the PUE bearing has a large vertical bearing capacity, promising horizontal deformability and energy dissipation capacity.

Another improvement to the elastomeric bearing has been recently proposed by Tan et al. (2022). In their publication, the authors discussed the development of a new elastomeric laminated bearing utilizing a core-and-filler system instead of a lead core to improve bearing performance. Two types of filler, namely granular and shape memory

polymer, are implemented. Granular filler is prepared using silica sand, while shape memory polymer filler is prepared using epoxy resin. Also, a steel core is implemented to improve the stiffness of the filler. The performance of the proposed bearing utilizing the core-and-filler system is evaluated using finite element simulation. The numerical results revealed the efficiency of bearing with the proposed system by providing considerable damping and stiffness. The replacement of lead core with filled granular and shape memory polymer showed improvement in terms of stiffness, proving that the core-and-filler system effectively limits lateral displacement. Also, the prototype of base isolation devices with both granular and shape memory polymer fillers is fabricated and tested via cyclic shear test. The results are compared with finite element analysis results, and good agreement between experimental tests results and numerical simulation response is shown. The experimental testing results proved that implementing the core-and-filler system improves the lateral resistance of the proposed elastomeric bearing. Overall, it can be concluded that the implementation of the core-and-filler system provides a reliable improvement to the performance of conventional elastomeric bearing and can be considered as an alternative system to lead core rubber bearings.

Kumar and Whittaker (2018) discussed the importance of verifying and validating mathematical models of elastomeric seismic isolation bearings and presented a plan for doing so. The authors noted that advanced models of elastomeric seismic isolation bearings were implemented in three commercial software packages (OpenSees, ABAQUS, LS-DYNA) and that these models were verified and validated per ASME best practices and guidelines. The authors further noted that the component of the mathematical model that contributes most to the error is the heating of the lead core in the LRB device and that code-to-code verification shows good agreement between the three software packages. Verified models were first calibrated using experimental data to determine unknown model parameters and to characterize the behavior of elastomeric bearings in tension and tension/shear.

Buckling is a phenomenon that causes instability to structural elements (Schilling and Mittelstedt 2020) when not addressed during the design stage. Rahnvard et al. (2020) used finite element analysis to investigate the stability of seismic steel-rubber base isolators. They looked at the effect of single and multiple rubber cores on the stability of elastomeric bearings and found that the use of single and multiple rubber cores increases isolator stability due to the large critical vertical loads. They also found that the equations presented in the reduced area formula provide the same stability results for isolators with and without a core. By comparing all square and circular isolator models with four and nine rubber cores (with the same core area), no noticeable difference in their stability was found. Kazeminezhad et al. (2020) have also used finite element analysis. The authors discussed rotation effects on the vertical stiffness of elastomeric bearings. It is found that rotation can increase the vertical stiffness of the isolator when the critical lateral displacement is reduced to a specific value. This information could help design base isolation systems.

Earlier studies on individual elastomeric bearings (Koh and Kelly 1987; Aiken et al. 1989; Naeim and Kelly 1999) showed that these bearing devices exhibit a reduction in their lateral stiffness under increasing vertical compressive loads. Additionally, experiments conducted by Kelly et al. on LSF (low shape factor) elastomeric (Aiken

et al. 1989) showed that load-history has a negligible effect on damping behavior of bearings and has some effect on reducing stiffness; however, the effect of loading rate on the response of the bearings was not significant (Aiken et al. 1989). In the same test program, Kelly et al. observed an increasing stiffness at large strains (over 125−150 %, which was demonstrated by the strain hardening characteristic of the elastomer. Furthermore, the vertical stiffness was found to be largely independent of any horizontal displacement imposed on the bearing (Aiken et al. 1989).

The author has observed some contradictions in results published by researchers in a wide range of documents; as an example, in the EERC-04-03 research report (Kelly and Takhirov 2004), Kelly et al. mentioned that:*"...the theory also predicts that the vertical stiffness of the bearing is strongly dependent on the shear deformation... The theoretical vertical stiffness significantly decreases as the shear deformation of the bearing increases"* this contradicts what was mentioned before in the EERC-89-13 research report (Aiken et al. 1989). However, some of the contradicted results may be due to the type of the bearing device itself and material properties from bearing to the bearing; any generalization of results should be with careful attention. In some tests, rubber bearings have been observed shown to soften in the vertical direction at large lateral deformations (Ryan and Chopra 2005). In some tests of pure tension, rubber bearings tend to cavitate or form small cavities in the rubber that blow out from negative pressure and link together to form cracks in the rubber matrix (Ryan and Chopra 2005), but other tension tests showed that no damage of this kind had been observed.

The characteristic strength of Lead Rubber Bearings (LRB), defined as the maximum force at zero horizontal bearing displacement, has been observed to increase with the increasing vertical (axial) load on the bearing but decreases from cycle to cycle; this is what was observed under a constant low-speed test (Benzoni and Casarotti 2008). The energy dissipated per cycle is related to the characteristic strength.

Several models were proposed for stability analysis of elastomeric bearings, among them, the linear models based on the Haringx theory developed by Koh and Kelly and its nonlinear version (Koh and Kelly 1987; Aiken et al. 1989), the two-spring models (Koh and Kelly 1987; Aiken et al. 1989) and the partially nonlinear extension of the two-spring model developed by Ryan (2005).

In this paper, an extension to the nonlinear extension of the two-spring model proposed by Ryan (2005) to the original model developed by Koh and Kelly (1987) is presented first. Then, two new fully nonlinear models suitable for elastomeric bearings and lead-rubber bearings are proposed to adequately account for the interaction between the horizontal and vertical loads. The accuracy of the models is verified using laboratory tests by Koh and Kelly (1988, 1987), Buckle et al. (2002), Warn et al. (2007).

Moreover, the effect of the interaction on the bearing's response parameters (horizontal stiffness, vertical stiffness, and overall stability) is investigated. Next, based on Hill's equation (Hill 1910), analytical models are then developed to predict the horizontal and vertical stiffnesses as a function of the critical buckling load. The two proposed mathematical models can readily be incorporated into open-source structural analysis software, such as OpenSees.

(a) Lead rubber bearing under test by mageba, Switzerland

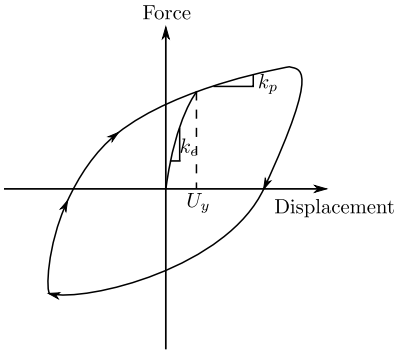

(b) force-displacement behavior in the horizontal direction

Fig. 3 Lead rubber bearing behavior in shear

2 Elastomeric bearing design parameters

For the design of elastomeric bearings, some design parameters are required to be determined, the most important are as itemized by Aiken et al. (1989) and Naeim and Kelly (1999):

- The horizontal stiffness of the bearing (k_h)
- The vertical stiffness of the bearing (k_v) and
- Stability of the bearing under combined vertical load and lateral displacement.

For elastomeric bearings with lead core, it is required in addition to the above, the determination of the characteristic strength of the lead, which is defined as the intercept (in the bilinear idealization model) of the hysteresis loop and the force axis (see Fig. 3), this parameter can be accurately estimated from the yield stress of the lead and lead-plug area (Naeim and Kelly 1999). Based on the linear analysis developed by Koh and Kelly (1987), Aiken et al. (1989), Kelly and Takhirov (2004), Naeim and Kelly (1999), the definition of the aforementioned design parameters is presented next.

2.1 Horizontal (shear) stiffness

The horizontal stiffness is defined by Naeim and Kelly (1999) as the most important mechanical property of the elastomeric bearing, it is given by:

$$k_h = \frac{GA}{t_r} \tag{1}$$

where G is the shear modulus of the elastomer, A is the full cross-sectional area, and t_r is the total rubber thickness. Note that Eq. 1 neglects the flexural deformation in comparison with shear deformation (Aiken et al. 1989).

2.2 Vertical (compression) stiffness

The vertical stiffness of the elastomeric bearing is given by (Naeim and Kelly 1999):

$$k_v = \frac{E_c A}{t_r} \tag{2}$$

where A may be taken as the area of shim plates and E_c is the instantaneous compression modulus of the rubber-steel composite under specified level of vertical load and it is related to the shape factor S, which is defined as the loaded area to force-free area ratio:

$$S = \frac{\Phi}{4\,t} \quad \text{for circular pad of diameter } \Phi \text{ and thickness } t \tag{3}$$

$$= \frac{a}{4\,t} \quad \text{for a square pad of side dimension } a \text{ and thickness } t \tag{4}$$

E_c for a single circular pad is given by:

$$E_c = 6GS^2 \tag{5}$$

and for a square pad, E_c is given by:

$$E_c = 6.73GS^2 \tag{6}$$

For LSF (Low Shape Factor) bearings, several formulae were proposed to determine the compression modulus (Aiken et al. 1989).

2.3 Maximum shear strain

The maximum shear strain γ is the parameter that controls the maximum horizontal displacement, D, and it is defined as:

$$\gamma = \frac{D}{t_r} \tag{7}$$

2.4 Stability —buckling load

Based on the Haringx theory developed for columns with low shear stiffness and adapted by Gent for rubber bearings, the buckling load of a bearing, taking into account the shear and flexural stiffnesses is expressed as (Aiken et al. 1989):

$$P_{cr} = \frac{P_S}{2}\left[\left(1 + 4\frac{P_E}{P_S}\right)^{1/2} - 1\right] \tag{8}$$

where

$$\begin{aligned} P_S &= GA_s \\ A_s &= A\frac{h}{t_r} \end{aligned} \tag{9}$$

$$P_E = \pi^2 \frac{EI_{eff}}{h^2} \tag{10}$$

and EI_{eff}=0.329E_cI (Naeim and Kelly 1999), I being the bearing moment of inertia. For shape factors in the range of 5−10, typical of isolation bearings, and for circular bearings with radius R and height h, ratio of P_S and P_E is given by (Aiken et al. 1989):

$$\frac{P_E}{P_S} = \frac{2h^2}{\pi^2 R^2 S^2} \tag{11}$$

An approximation for P_{cr} is given by (Aiken et al. 1989):

$$P_{cr} = \sqrt{P_S P_E} \tag{12}$$

considering that most bearings are quite squat with $h \cong R$. Substituting Eqs. 9 and 11 into Eq. 12 yields (Naeim and Kelly 1999):

$$P_{cr} = \frac{\sqrt{2} GASr}{t_r} \tag{13}$$

where the radius of gyration is denoted by $r = \sqrt{\frac{I}{4}} = \frac{a}{2\sqrt{3}}$ for a square bearing with side dimension a and $\Phi/4$ for a circular bearing with diameter Φ. A correction coefficient was proposed later by Stanton and Roeder (Komodromos 2000), it is given by:

$$f_r = B_r S^2 \tag{14}$$

where B_r=0.742 for a square bearing and 0.5 for a circular one. Therefore, the buckling load which may be used for a stability check of a circular bearing is given by (Komodromos 2000):

$$P_{cr} = \frac{0.134 G \Phi^5}{t_r t^2} \tag{15}$$

where t is the thickness of a single rubber shim.

3 Nonlinear extension of the two-spring model (Ryan and Chopra 2005)

Since most isolation bearings are inherently nonlinear, especially LRB due to the yielding of the lead core, a nonlinear extension of the linear two-spring model (Koh and Kelly 1987) was proposed by Ryan et al. (2005) which includes various constitutive models for the shear spring. The nonlinear model considers a linear vertical spring to account for the axial load effects, however, as an option a model for strength of lead degradation was incorporated to the *coupled nonlinear variable strength model* (Ryan and Chopra 2005), in fact, this model (model for strength degradation) is an empirical equation for yield strength Q as a function of the compression load P and it is based on experimental data, it is given by (Ryan and Chopra 2005):

$$Q = Q_0 \left(1 - e^{-P/P_0}\right) \tag{16}$$

where Q_0 is the nominal yield strength of the bearing, achievable with an adequate confining pressure, and P_0 is the axial (vertical) load corresponding to about 63% of nominal strength (Ryan and Chopra 2005).

The problem with Eq. 16 is that values of Q_0 and P_0 are difficult to be determined. It would be interesting to develop a model that needs only the mechanical and geometric properties instead of using parameters from response behavior. The nonlinear extension of the two-spring model considers a constant initial (i.e., elastic) stiffness, so that will not undergo a reduction or increase when applying axial loads. The model proposed by Ryan is based on the illustration shown in Fig. 4, in this model the shear spring is no more linear as in the two-spring model, it has been replaced by a general force $f_s(s)$. The equilibrium equations relating the lateral force f_b (see Fig. 4) and the axial (compressive) force P to f_s and the small rotation θ through the rotational spring are as follows:

$$f_b - f_s(s) + P\theta = 0 \tag{17}$$

$$f_b h_b - P_E h_b \theta = 0 \tag{18}$$

$$P - k_{bz0} v = 0 \tag{19}$$

where k_{bz0} is the vertical stiffness of the linear vertical spring (not shown in Fig. 4 and v being the associated vertical spring elongation (i.e., deformation).

The kinematic equations relating the total lateral displacement, u_b, and vertical deformation, u_{bz}, to the internal deformations, s, θ and v (assuming small rotation θ) are:

$$\begin{aligned} u_b &= s + h_b\theta \\ u_{bz} &= v + \delta_{bz} \end{aligned} \tag{20}$$

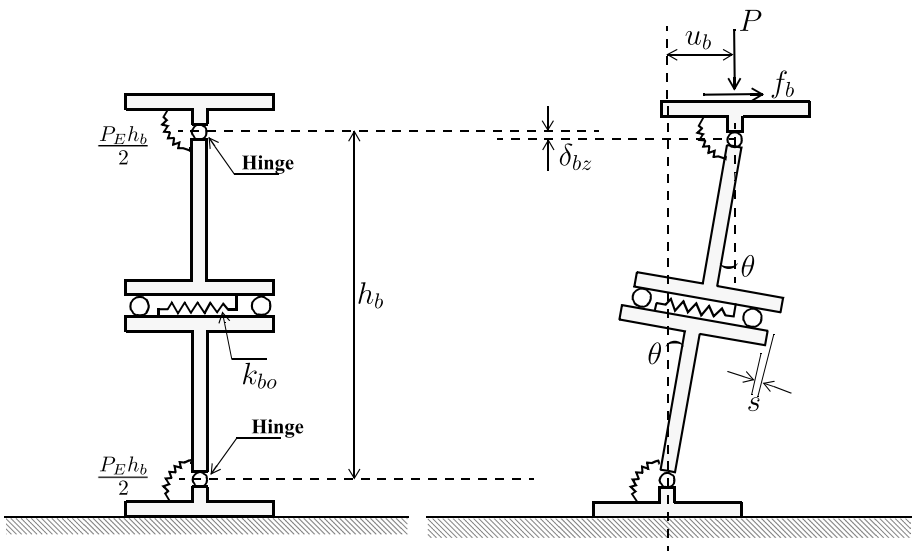

Fig. 4 Two-spring model of an isolation bearing in the undeformed and deformed configuration (Source: (Ryan and Chopra 2005))

$$= v + s\theta + \frac{h_b}{2}\theta^2 \tag{21}$$

in which u_{bz} is positive in compression and δ_{bz} is the additional vertical displacement that occurs in the laterally-deformed configuration (see Fig. 4).

Equations 17 to 20 can be written in the following compact from:

$$\boldsymbol{g} = \begin{Bmatrix} g_1 \\ g_2 \\ g_3 \\ g_4 \\ g_5 \end{Bmatrix} = \begin{Bmatrix} f_b - f_s(s) + P\theta \\ f_b h_b - P_E h_b \theta + P(s + h_b\theta) \\ P - k_{bz0} v \\ u_b - s - h_b\theta \\ u_{bz} - s\theta - \frac{h_b}{2}\theta^2 - v \end{Bmatrix} \tag{22}$$

The above system of equations may be solved using the Newton's method, i.e., find $\boldsymbol{x}=\langle f_b,P,s,\theta,v\rangle^T$ to satisfy $\boldsymbol{g(x)=0}$. A bearing flexibility matrix $\boldsymbol{f_b}$ relating the bearing forces $\boldsymbol{dF}=\langle df_b,dP\rangle^T$ to the change in deformation $\boldsymbol{dU}=\langle du_b,du_{bz}\rangle^T$ it is given after Ryan (2005) as follows:

$$\boldsymbol{f_b} = \begin{Bmatrix} \frac{(P_E+P)h_b+h_b^2(\partial f_s/\partial s)}{h_b(\partial f_s/\partial s)(P_E-P)-P^2} & \frac{P_E h_b\theta+[P+h_b(\partial f_s/\partial s)](s+h_b\theta)}{h_b(\partial f_s/\partial s)(P_E-P)-P^2} \\ \frac{P_E h_b\theta+[P+h_b(\partial f_s/\partial s)](s+h_b\theta)}{h_b(\partial f_s/\partial s)(P_E-P)-P^2} & \frac{(P_E+P)h_b\theta^2+2Ps\theta+(\partial f_s/\partial s)(s+h_b\theta)^2}{h_b(\partial f_s/\partial s)(P_E-P)-P^2} + \frac{1}{k_{bz0}} \end{Bmatrix} \tag{23}$$

The complexity of Eq.23 is evident because the bearing stiffness matrix, $\boldsymbol{k_b}$ (i.e., inverse of $\boldsymbol{f_b}$) is not derived explicitly.

4 Proposed alternative nonlinear extension models

The nonlinear extension of the two-spring model (Ryan and Chopra 2005) considers the vertical stiffness of the bearing as elastic and constant and the strength variation was an empirical equation incorporated in the model using Eq.16. However, Ryan's model predicts accurately the strength variation with axial loads and the horizontal stiffness degradation with increasing axial loads.

Based on the need for fast prediction of the response behavior of elastomeric bearings under different load cases, two models are proposed. The models are suitable to predict the behavior (static case only) of elastomeric bearings and especially the lead rubber bearings. The first model, referred to herein as the *first alternative nonlinear extension model*, includes nonlinear shear spring with a simpler constitutive equation that works in the case of positive lateral monotonic loading while the vertical spring is kept linear as in the two-spring model. The second model, referred to herein as the *second alternative nonlinear extension model* is similar to the first alternative model but the vertical spring is nonlinear and it is represented by a general force. The two alternative models account directly for strength variation and elastic stiffness variation under combined axial and lateral loads.

4.1 First alternative nonlinear extended model

In this model the shear spring is represented by a nonlinear mobilized force, $f_s(s)$, given by the following equation:

$$f_s(s) = k_{b0}s + Q_0 z \tag{24}$$

Considering that the bearing will undergo only positive displacements as in the case represented by Fig. 4 and considering only static analysis of the bearing behavior, the dimensionless parameter z in this case is governed by the following equation:

$$z = 1 - e^{-s/s_y} \tag{25}$$

s_y being the yield shear displacement. At yielding z approaches $+1$ and the term e^{-s/s_y} approaches *zero*. The differential of the mobilized force in the shear spring, $f_s(s)$, will be:

$$\frac{df_s}{ds} = k_{b0} \tag{26}$$

Substituting Eq.26 in the term f_{11} from the flexibility matrix given in Eq. 23 yields:

$$\begin{aligned} f_{11} &= \frac{(P_E+P)h_b+h_b^2k_{b0}}{P_SP_E-PP_S-P^2} \\ &= \frac{(P_E+P)h_b+h_b^2k_{b0}}{P_SP_E-PP_S-P^2} \end{aligned} \tag{27}$$

At buckling condition, the stiffness k_{b11}, the inverse of f_{11}, equals zero if:

$$P_SP_E - PP_S - P^2 = 0 \tag{28}$$

The solution of Eq. 28 assuming that $P_E >> P_S$ yields the critical load $P_{cr} = \sqrt{P_E P_S}$ (Naeim and Kelly 1999). Note that Eq.27 was achieved assuming the bearing at the post-elastic state, however, Ryan and Chopra (2005) considered that the shear spring is linear to achieve at the same equation.

The governing equations (Eq. 17 to 20) are unchanged, leading to the system of non-linear equations, Eq. 22). Substituting Eq. 25 in Eq. 24 and Eq. 24 into Eq. 22 yields:

$$\boldsymbol{g} = \begin{Bmatrix} g_1 \\ g_2 \\ g_3 \\ g_4 \\ g_5 \end{Bmatrix} = \begin{Bmatrix} f_b - [k_{b0}s + Q_0(1 - e^{-s/s_y})] + P\theta \\ f_b h_b - P_E h_b \theta + P(s + h_b\theta) \\ P - k_{bz0}\nu \\ u_b - s - h_b\theta \\ u_{bz} - s\theta - \frac{h_b}{2}\theta^2 - \nu \end{Bmatrix} \tag{29}$$

Considering the axial load, P, and the bearing lateral displacement, u_b, as input parameters, the vector of unknowns is then $\boldsymbol{x}=\langle f_b,s,\theta\rangle^T$, which are needed to be determined to satisfy $\boldsymbol{g(x)=0}$,$\boldsymbol{g}$ in this case is a system of only four equations with three unknowns.

$\boldsymbol{g(x)=0}$ is solved using the Newton's method following the next step-by-step procedure:

1. Calculate the function values at the guessed value of $\boldsymbol{x^i}=\langle f_{b1},s_1,\theta_1,\rangle^T$
2. Calculate the Jacobian matrix using the current guess for the solution
3. Solve the linear system $-\boldsymbol{g(x^i)}=\boldsymbol{Jdx}$ for the values of $\boldsymbol{dx}$
4. Update the guessed value $\boldsymbol{x^{i+1}}=\boldsymbol{x^i}+\boldsymbol{dx}$

This procedure should be repeated, using the updated value of $\boldsymbol{x}^i$ as the guess, until the values of $\boldsymbol{g(x)}$ are sufficiently close to zero. $\boldsymbol{g(x)}$ is a vector of ***residual errors***, which can be considered close to zero when:

$$\max\left[g_1(x), g_2(x), g_3(x)\right] < \text{Tolerance} \tag{30}$$

or the 2−norm of the vector $\boldsymbol{g(x)}$,

$$\|\boldsymbol{g}(\boldsymbol{x})\| = \left(\sum_{i=1}^{3} g_i^2\right)^{1/2} \tag{31}$$

The Jacobian matrix if the matrix of derivatives:

$$J = \begin{bmatrix} \partial g_1/\partial f_b & \partial g_1/\partial s & \partial g_1/\partial \theta \\ \partial g_2/\partial f_b & \partial g_2/\partial s & \partial g_2/\partial \theta \\ \partial g_3/\partial f_b & \partial g_3/\partial s & \partial g_3/\partial \theta \end{bmatrix} \tag{32}$$

The Jacobian matrix should be non-singular because in this case Newton's method will fail. Therefore, the solution of $\boldsymbol{g(x)=0}$ becomes a minimization problem.

4.2 Second alternative nonlinear extended model

The second alternative nonlinear extension model has the same mobilized force representation of the shear spring, but differs in the behavior of the vertical spring. The second model includes a nonlinear vertical spring represented by another mobilized force.

Experiments on elastomeric bearing isolators (Koh and Kelly 1987) showed that the height reduction of the bearing is nonlinearly related to the increase of axial compressive load. Based on these experimental data, an equation that governs the behavior of the vertical spring is proposed, it is given by:

$$v = \frac{1}{k_{pz0}} P + v_y(1 - e^{-P/P_y}) \tag{33}$$

where k_{pz0} is the post-elastic stiffness of the vertical spring, v_y is the yield vertical deformation and P_y is the corresponding yield compressive load (see Fig. 5). Substituting Eq. 33 in the system of Eqs. 29 leads to a new system of equations $\boldsymbol{g(x)=0}$ which can be solved using the same algorithm presented before. It should be noted that only positive (compressive) axial loads are taken into consideration in Eq. 33.

5 Behavior of lRB via new models

In what follows the response behavior of a LRB is investigated under two different load cases:

- Monotonic lateral displacement (i.e., increasing u_b) combined with a wide range of axial compressive loads, P.
- Monotonic vertical Loading (i.e., increasing compression P) combined with a wide range of lateral positive displacement, u_b.

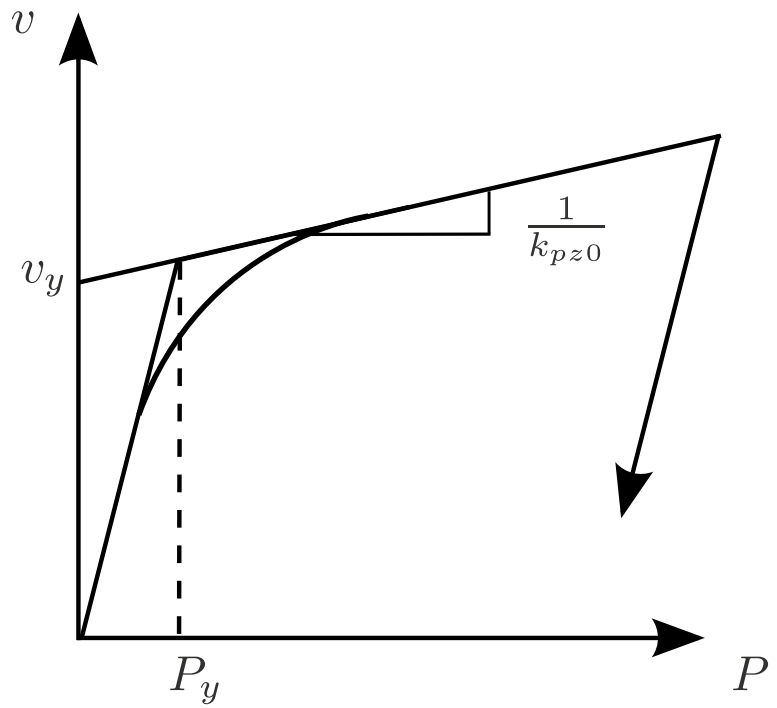

Fig. 5 Nonlinear model of the vertical spring

Table 1 Geometric and mechanical properties of the LRB

Parameter	Value
Total bearing height, h_b	200 mm
Bearing diameter, Φ_r	216 mm
Total rubber thickness, t_r	133.3 mm
Rubber shear modulus, G_r	0.73 MPa
Lead diameter, Φ_l	38.1 mm
Lead shear modulus, G_l	130 MPa
Lead shear stress, τ_l	10.5 MPa
Estimated yield shear deformation, s_y	10 mm

The response parameters of interest are:

- Variation of elastic stiffness, k_{be}
- Variation of post-elastic stiffness, k_{bp}
- Variation of effective stiffness, k_{beff}
- Variation of maximum bearing height
- Variation of vertical stiffness, k_{bz}

The characteristics of the LRB are given in Table 1. For the second alternative nonlinear extension model, the axial deformation-axial load relationship, determined based on experimental data, is defined through the parameters:

- k_{pz0}=5.1 10^4 kN/m ^{2}
- v_y=2.83 mm
- P_y=51.17 kN

5.1 Monotonic increased horizontal displacement under constant axial load

For this load case, the bearing is subjected to a monotonically increasing horizontal displacement u_b up to 127 mm (displacement-controlled) under a constant compression P. A number of such analysis was performed with varying compression loads so as to study the effect of the compression load on the behavior of the bearing. As the proposed models are specialized for static analysis, the 1/4 cycle portion of the hysteresis loop of the horizontal mobilized force versus horizontal displacement is obtained in each of the analyses (Fig. 6).

As shown in Fig. 6, the effect of axial compression load is clear; under compression, the bearing shows a decrease in both elastic and post-elastic stiffness. The critical buckling load can be estimated from the figure to be $P_{cr}\approx$250 kN; at this compression level, the post-elastic stiffness approaches *zero*. Eq. 12 predicts the critical buckling load as P_{cr}=269.74 kN. The proposed alternative model agrees well with the approximate equation proposed by Naeim and Kelly (1999).

5.1.1 Variation of horizontal stiffness

Variation of the horizontal elastic stiffness and post-elastic stiffness with axial compressive load are presented in Fig. 7a and b.

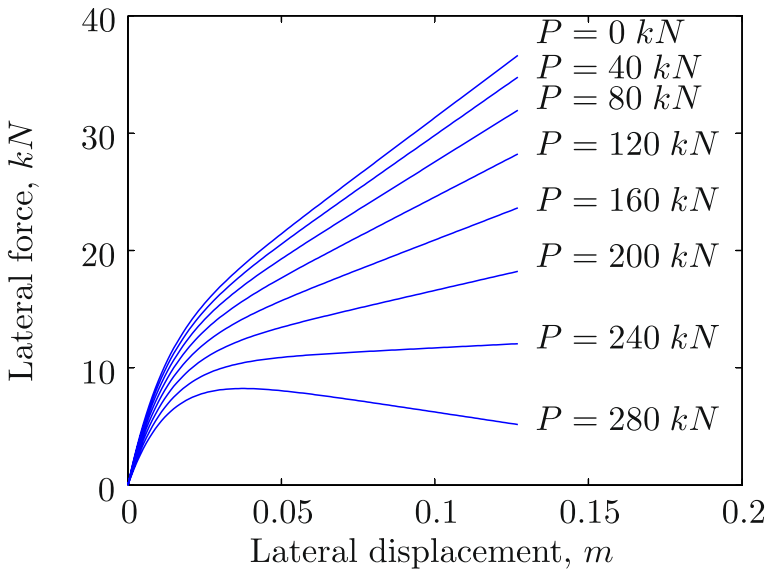

Fig. 6 Lateral force-lateral displacement trends under different compressive loads

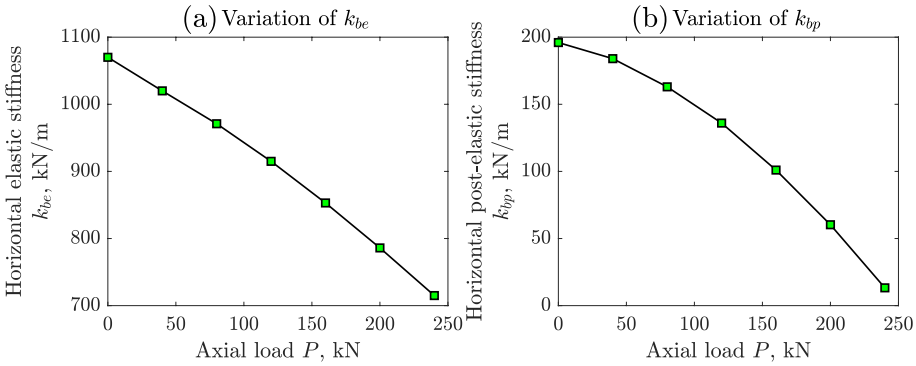

Fig. 7 Variation of horizontal pre- and post-elastic stiffness with axial compression load

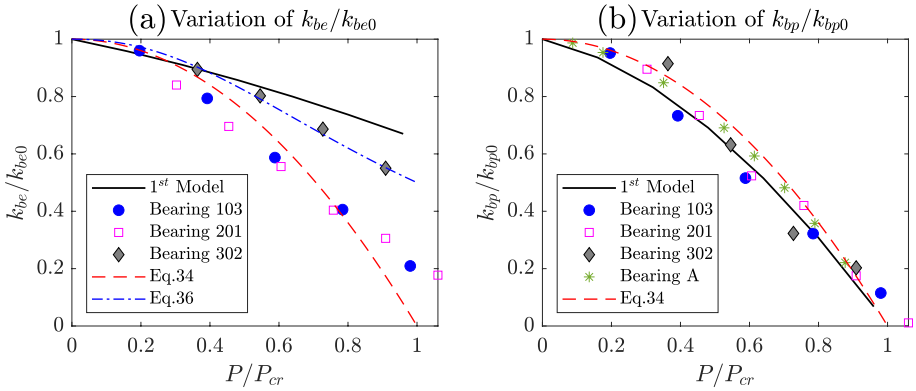

Fig. 8 Variation of normalized horizontal pre- and post-elastic stiffness with axial compression load

Clearly, the horizontal post-elastic stiffness decreases significantly with the increase in axial load, however, the decrease that the horizontal elastic stiffness undergoes is less rapid and it is approximately linear.

Figure 8a and b show the normalized horizontal elastic stiffness (k_{be}/k_{be0}), respectively, the normalized post-elastic stiffness (k_{bp}/k_{bp0}) as a function of the normalized axial load (P/P_{cr}). k_{be0} and k_{bp0} are the horizontal elastic stiffness and horizontal post-elastic stiffness at zero axial load, respectively. In addition to the results of the mathematical model, Fig. 8 includes also experimental results carried out by Koh and Kelly (1987, 1988) (Bearing A) and Buckle et al. (2002) (Bearings 103, 201, and 302). These experiments demonstrate the reliability of the proposed mathematical models in predicting the variation of the horizontal stiffness of lead rubber bearings with the axial load.

Naeim and Kelly (1999) proposed an equation that approximates the relationship between the horizontal post-elastic stiffness and axial load, it is given by:

$$k_{bp} = k_{bp0}\left[1 - \left(\frac{P}{P_{cr}}\right)^2\right] \tag{34}$$

Equation 34 is accurate if the load is less than 0.32 times the buckling load (Naeim and Kelly 1999).

The theoretical curves for the normalized elastic and post-elastic horizontal stiffness versus P/P_{cr} based on the first model and Eq.34 are shown in Fig. 8a and b.

It can be seen that the first model predicts the significant decrease of horizontal post-elastic stiffness with axial load as Eq.34 (Fig. 8b), a good check on the model's accuracy.

Based on Hill's equation (Hill 1910), a new analytical approximation is proposed to fit the model and test results. The Hill (or Hill-Langmuir) equation was proposed by A. Hill in 1910 to describe the sigmoidal oxygen binding curve of hemoglobin (Hill 1910). The general form of Hill's equation is given by:

$$y = \frac{y_{max}}{1 + \left(\frac{x}{x_r}\right)^{\alpha}} \tag{35}$$

In wichh, x_r is the reference coefficient, which produces $y{=}y_{max}/2$; y_{max} is the upper asymptote; α is the Hill coefficient. When the hill coefficient is greater than 1.0, Hill's curve will have an inflection point.

The proposed approximation to the variation of the normalized elastic stiffness is given by:

$$k_{be} = k_{be0}\left[\frac{1}{1 + \left(\frac{P}{P_{cr}}\right)^{2.2}}\right] \tag{36}$$

In Eq. 36, the maximum elastic stiffness (i.e., upper asymptote) is equal to the stiffness at zero axial loads, k_{be0}, and the reference coefficient is equal to 1.0. The Hill coefficient is equal to 2.2 and this means that the curve's inflection point takes place at much higher values of P/P_{cr}. Figure 8a shows that the proposed approximation is reasonably accurate compared to part of the test data. The same Figure also shows that when Eq. 34 is specialized for the elastic stiffness instead of the post-elastic stiffness, it can be a good approximate to some of the test data, especially for values of $P/P_{cr}{\leq}0.8$.

The horizontal effective stiffness undergoes a reduction with increased axial loads, this decrease is less significant as the decrease of horizontal post-elastic stiffness and more significant as compared with the decrease of the horizontal elastic stiffness. When P

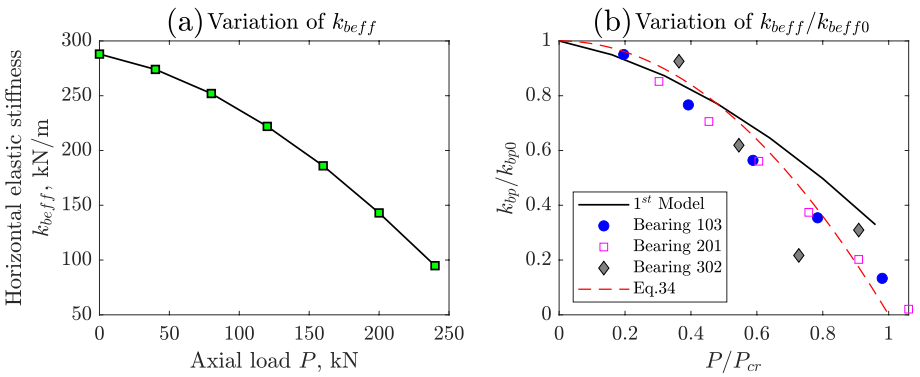

Fig. 9 Variation of horizontal effective stiffness with axial compression load

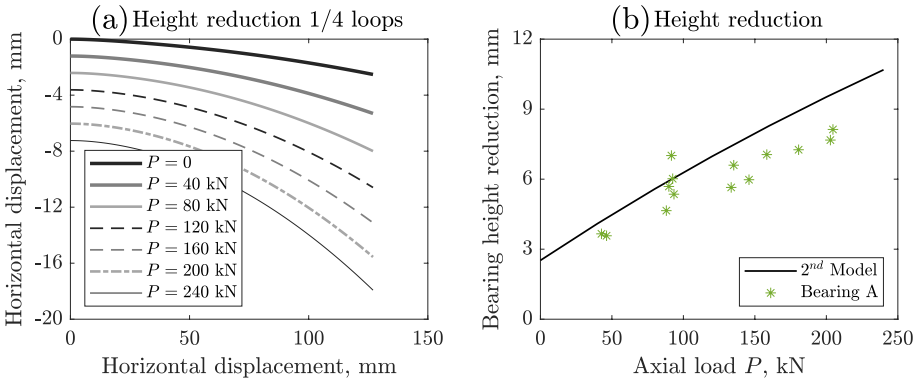

Fig. 10 Variation of height reduction with axial compression load

approaches P_{cr} the effective stiffness decreases to approximately 1/3 of the effective stiffness at zero axial load (see Fig. 9a).

From Fig. 9b it is clear that the first model agrees well with the approximation predicted by Eq.34 when specialized for effective stiffness.

5.1.2 Variation of vertical displacement

Figure 10a plots the vertical displacement of the top of the bearing with lateral displacement under different axial loads, and Fig. 10b plots variation of maximum height reduction (calculated as the difference between maximum and minimum vertical displacements) with the variation of axial load. The figures demonstrate that the bearing under the considered load case deforms in *arc-shape* configuration; the increase in compressive axial load decreases the height of the bearing. The bearing under near buckling load will have the shape of an arc of a circle with smaller radius of curvature.

Figure 10b shows in addition the response of Bearing A tested by Koh and Kelly (1988). Compared to these tests, the model demonstrates its capability of capturing well the overall vertical displacement of the bearing under increasing axial loads.

5.1.3 Variation of vertical stiffness

For the first load case, the reduction of the bearing height with increasing axial load does not always mean that the vertical stiffness increases as well. The variation of the bearing normalized vertical stiffness (normalization by the initial vertical stiffness) with the horizontal displacement under different levels of axial load is shown in Fig. 11. The bearing vertical stiffness decreases rapidly under increasing horizontal displacement and constant axial compression load.

5.2 Monotonic increasing axial load under constant shear strain

For this load case, the bearing is subjected to a monotonically increasing axial compressive load P up to 240 kN (force-controlled) under a constant horizontal displacement u_b. A number of such analysis was performed with varying compression loads so as to study

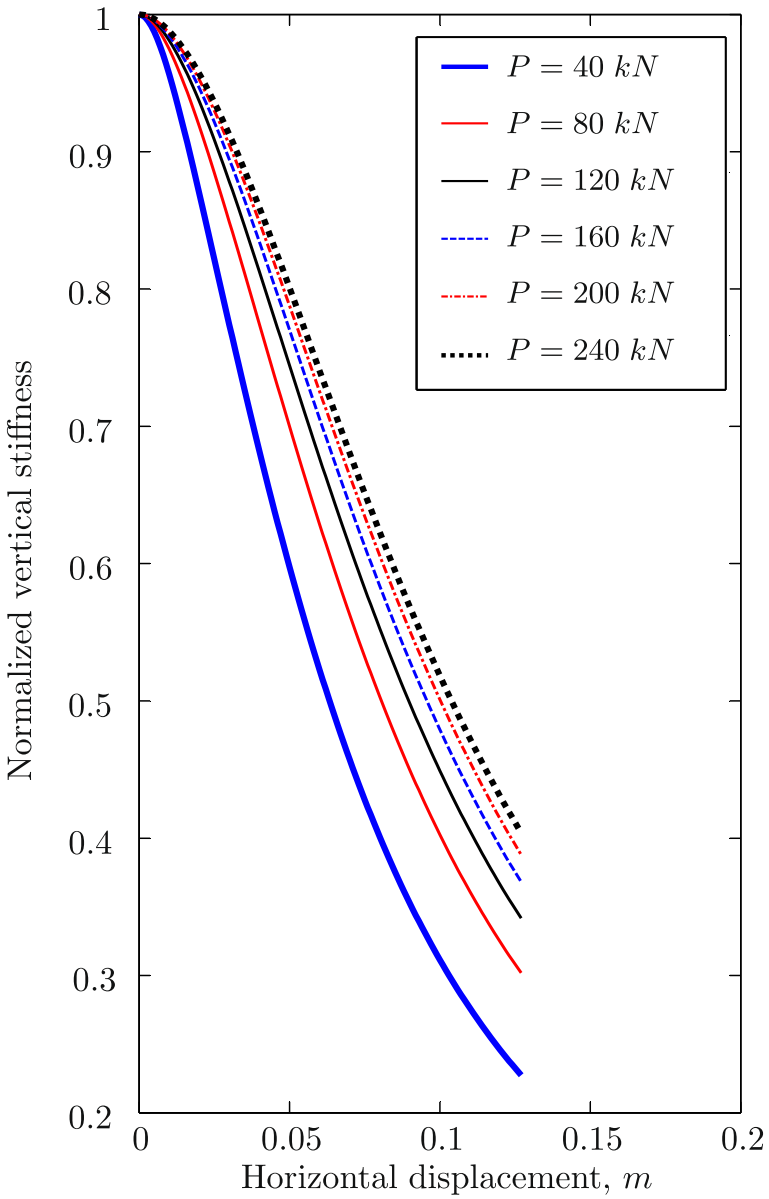

Fig. 11 Variation of vertical normalized stiffness with horizontal displacement

the combined effect of the compression load and shear strain on the vertical stiffness of the bearing.

Figure 12a plots the axial load versus the vertical displacement curves under different maximum shear strain while Fig. 12b plots the variation of normalized vertical stiffness with shear strain. Under constant axial load, the vertical displacement of the top of the bearing increases with increasing shear strain. Additionally, when combined with axial compressive load, the maximum shear strain causes a considerable reduction in the vertical stiffness, however, the effect of maximum shear strain is more significant than the effect of axial load.

Compared to experimental results by Warn et al. (2007), Fig. 12b demonstrates that the 2nd model can be accurate in predicting the variation of the vertical bearing stiffness

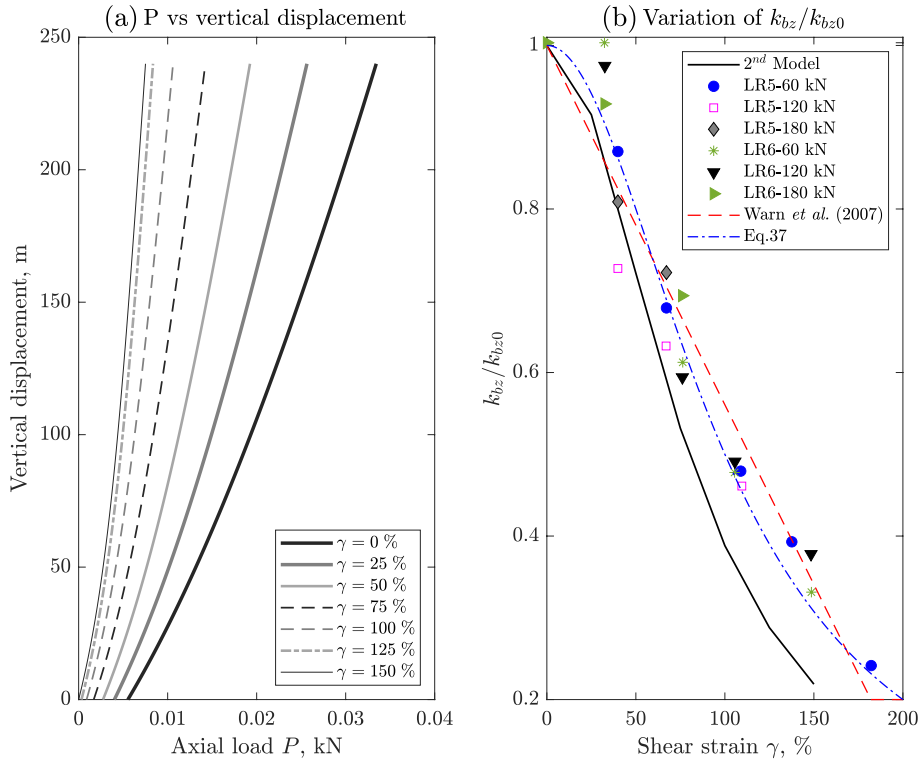

Fig. 12 Axial load versus vertical displacement curves and variation of normalized vertical stiffness with shear strain

with the shear strain. Moreover, it is observed that if the effect of the axial load is neglected, the decrease in the vertical stiffness can be approximated by:

$$k_{bz} = k_{bz0}\left[\frac{1}{1+\gamma^2}\right] \tag{37}$$

Equation 37 is again a Hill equation with a reference coefficient equal to 1.0 and Hill coefficient equal to 2.0. As shown in 12b, the analytical model defined by Eq. 37 can be a good approximation to the variation of the vertical stiffness of the lead rubber bearings. Note that the figure shows, in addition, the simple, yet accurate, approximation proposed by Warn et al. (2007) (Eq. 21 in the reference).

6 Summary and conclusions

This study proposed two alternative nonlinear extensions for the original two-spring model. The proposed models are fully nonlinear and developed to predict the behavior of elastomeric bearings and lead rubber bearings under different load cases. Both models consider the interaction between the horizontal and vertical loads. The investigation has led to the following conclusions:

1. Comparisons between laboratory tests and the proposed models demonstrated that the models are capable of accurately replicating the behavior of lead rubber bearings.

2. The horizontal post-elastic stiffness decreases significantly as axial load increases.
3. The decrease that the horizontal elastic stiffness undergoes under increasing axial compression load is less rapid than the decrease in horizontal post-elastic stiffness.
4. The effective horizontal stiffness undergoes a reduction with increased axial loads, this decrease is less rapid as the decrease of horizontal post-elastic stiffness and more rapid as compared with the decrease of horizontal elastic stiffness; when P approaches P_{cr} the effective stiffness decreases to approximately 1/3 of the effective stiffness at zero axial loads.
5. The vertical stiffness of an elastomeric bearing rapidly decreases as horizontal displacement increases.
6. Under a constant axial load, the vertical displacement of the top of the elastomeric bearing increases with increasing shear strain.
7. The maximum shear strain combined with axial compressive load reduces the vertical stiffness considerably; however, the effect of maximum shear strain is more significant than the effect of axial loads.

The outcomes of this study include:

- An analytical model to predict the horizontal stiffness of lead rubber bearings as a function axial loads and critical buckling loads.
- An analytical model to predict the vertical stiffness of lead rubber bearings at different shear strain levels.
- Ready-to-implement mathematical models of elastomeric bearings and lead-rubber bearings into available finite element and structural analysis software.
- The proposed models may serve as a preliminary design tool (to select an isolation system before going through a full structural analysis) or as a final design checking tool (stability analysis after selecting the isolation system's geometric and mechanical properties).

On the limitations side, the proposed models do not incorporate strength variation with axial load; the two models predict approximately constant yield strength under increased axial compression loads. However, the strength at the onset buckling and post-buckling stages can be reliably captured by both models.

Acknowledgments
The second author is the former supervisor of the first author during his PhD studies, which were supported by the Romanian and Algerian governments. The present work is Partially supported by the University of Sharjah, UAE. These supports are highly acknowledged.

Authors' contributions
The author is the sole contributor to writing the manuscript. The author(s) read and approved the final manuscript.

Funding
The author received support from the Ministry of Higher of Education and Scientific Research, Algeria and partial support University of Sharjah, United Arab Emirates.

Availability of data and materials
Research-related data are contained within the manuscript.

Declarations

Competing interests
The authors declare that they have no competing interests.

Received: 13 May 2022 Accepted: 8 August 2022
Published online: 02 September 2022

References

Aiken, ID, Kelly JM, Tajirian FF (1989) Mechanics of Low Shape Factor Elastomeric Seismic Isolation Bearings. Berkeley, Calif: Earthquake Engineering Research Center, College of Engineering, University of California.
Benzoni, G, Casarotti C (2008) Performance of lead-rubber and sliding bearings under different axial load and velocity conditions. Report Number: SRMD -2006/05-rev3. https://rosap.ntl.bts.gov/view/dot/27663.
Buckle, I, Nagarajaiah S, Ferrell K (2002) Stability of elastomeric isolation bearings: Experimental study. J Struct Eng 128:3–11.
Graf, M, Lankenau T (2021) Viscous damping exciting friction-induced vibration in pin-on-disk systems. Results Eng 12:100299. https://www.sciencedirect.com/science/article/pii/S2590123021001006.
Hill, A (1910) The possible effects of the aggregation of the molecules of haemoglobin on its dissociation curves. J Physiol 40:4–7.
Ibrion, M, Paltrinieri N, Nejad A (2020) Learning from non-failure of Onagawa nuclear power station: an accident investigation over its life cycle. Results Eng 8:100185. https://www.sciencedirect.com/science/article/pii/S2590123020300931.
Kalpakidis, I, Constantinou M (2009) Effects of heating on the behavior of lead-rubber bearings. I: Theory. J Struct Eng 135:1440–1449.
Kalpakidis, I, Constantinou M (2009) Effects of heating on the behavior of lead-rubber bearings. II: Verification of theory. J Struct Eng 135:1450–1461.
Kalpakidis, I, Constantinou M, Whittaker A (2010) Modeling strength degradation in lead–rubber bearings under earthquake shaking. Earthquake Eng Struct Dyn 39:1533–1549.
Kazeminezhad, E, Kazemi M, Mirhosseini S (2020) Assessment of the vertical stiffness of elastomeric bearing due to displacement and rotation. Int J Non-Linear Mech 119:103306. https://doi.org/10.1016/j.ijnonlinmec.2019.103306.
Kelly, JM, Takhirov, S (2004) Analytical and Numerical Study on Buckling of Elastomeric Bearings with Various Shape Factors. Berkeley: Earthquake Engineering Research Center, University of California.
Koh, CG, Kelly JM (1987) Effects of Axial Load on Elastomeric Isolation Bearings. Berkeley, Calif: Earthquake Engineering Research Center, College of Engineering, University of California.
Koh, C, Kelly J (1988) A simple mechanical model for elastomeric bearings used in base isolation. Int J Mech Sci 30:933–943.
Komodromos, P (2000) Seismic Isolation for Earthquake Resistant Structures. WIT Press, Boston.
Kumar, M, Whittaker A (2018) Cross-platform implementation, verification and validation of advanced mathematical models of elastomeric seismic isolation bearings. Eng Struct 175:926–943. https://doi.org/10.1016/j.engstruct.2018.08.047.
Naeim, F, Kelly JM (1999) Design of Seismic Isolated Structures: From Theory to Practice. Wiley, New York.
Rahnavard, R, Craveiro H, Napolitano R (2020) Static and dynamic stability analysis of a steel-rubber isolator with rubber cores. Structures 26:441–455. https://doi.org/10.1016/j.istruc.2020.04.048.
Ryan, KL, Chopra AK (2005) Estimating the Seismic Response of Base-Isolated Buildings Including Torsion, Rocking, and Axial-Load Effects. Berkeley: Earthquake Engineering Research Center, University of California.
Schilling, J, Mittelstedt C (2020) A simple closed-form analytical model for the column buckling of omega-stinger-stiffened panels with periodic boundary conditions. Results Eng 6:100120. https://www.sciencedirect.com/science/article/pii/S2590123020300268.
Tan, K, Hejazi F, Esfahani H, Chong T (2022) Development of Elastomeric Rubber Bearing Utilizing Core-and-Filler System. Structures 37:125–139. https://doi.org/10.1016/j.istruc.2021.12.074.
Tsao, W, Huang Y (2021) Sloshing force in a rectangular tank with porous media. Results Eng 11:100250. https://www.sciencedirect.com/science/article/pii/S2590123021000517.
Warn, G, Whittaker A, Constantinou M (2007) Vertical stiffness of elastomeric and lead–rubber seismic isolation bearings. J Struct Eng 133(9):1227–1236. https://doi.org/10.1061/(ASCE)07339445(2007)133:9(1227), https://ascelibrary.org/doi/abs/10.1061/%28ASCE%290733-9445%282007%29133%3A9%281227%29.
Yuan, Y, Wang S, Tan P, Zhu H (2020) Mechanical performance and shear constitutive model study of a new high-capacity polyurethane elastomeric bearing. Construct Build Mater 232:117227. https://doi.org/10.1016/j.conbuildmat.2019.117227.

Publisher's Note